HHS Public Access

Author manuscript

J Occup Environ Hyg. Author manuscript; available in PMC 2024 September 01.

Published in final edited form as:

J Occup Environ Hyg. 2023 September ; 20(9): 390–400. doi:10.1080/15459624.2023.2227658.

Validation of N95 respirator models for pressure drop and particle capture efficiency

Patrick T. O'Shaughnessy[a,*], **Zoe Harris**[a], **Matthew Purdy**[a], **Ralph Altmaier**[a]

[a]Department of Occupational and Environmental Health, The University of Iowa, Iowa City, IA 52241

Abstract

Despite efforts to apply administrative and engineering controls to minimize worker exposure to aerosols, filtering facepiece respirators (FFRs) continue to be an important form of personal protective equipment in hard-to-control settings such as healthcare, agriculture and construction. Optimizing the performance of FFRs can be advanced with the use of mathematical models that incorporate the forces that act on particles during filtration as well as those filter characteristics that influence filter pressure drop. However, a thorough investigation of these forces and characteristics using measurements of currently-available FFRs has not been undertaken. Filter characteristics such as fiber diameter and filter depth were measured from samples taken from six currently-available N95 FFRs from three manufacturers. A filtration model was developed that included diffusion, inertial and electrostatic forces to estimate the filtration of an aerosol with a Boltzmann charge distribution. The diameter of the filter fibers was modeled as either a single "effective" diameter or as a lognormal distribution of diameters. Both modeling schemes produced an efficiency curve that simulated efficiency measurements made over a range of particle diameters (0.01 – 0.3 μm) with the use of a scanning mobility particle sizer in the region where efficiency is at a minimum. However, the method using a distribution of fiber diameters, produced a better fit for particles > 0.1 μm. The coefficients associated with a simple form of the diffusion equation constituting a power law incorporating the Peclet number were adjusted to enhance model accuracy. Likewise, the fiber charge of the electret fibers was also adjusted to maximize model fit but remained within levels reported by others. A filter pressure drop model was also developed. Results demonstrated the need for a pressure drop model applicable to N95s relative to existing models developed with the use of fibers with larger diameters than those used in current N95 FFRs. A set of N95 FFR characteristics are provided that can be used to develop models of typical N95 FFR filter performance and pressure drop in future studies.

Keywords

filtration; pressure drop; diffusion; fiber charge; respirator

[*]**Corresponding Author:** Patrick T. O'Shaughnessy | patrick-oshaughnessy@uiowa.edu.

INTRODUCTION

The recent pandemic emphasized the importance of the use of N95 filtering facepiece respirators (FFRs) in healthcare settings during which their supply was often at critically low levels. Use of an N95 FFRs by healthcare workers, or any other worker, is hampered by relevant issues such as the difficulty forming and maintaining an airtight seal that diminishes their "fit" against the face (Bergman et al. 2015), as well as factors associated with the perception of discomfort while worn, such as heat caused by exhaled breath, tightness against the face, and the additional effort required to breathe through the filter media layers of an N95 FFR (Fukakusa et al. 2011; Shaffer and Janssen 2015).

The pressure drop, or "breathing resistance," represents a critical design feature of an N95 FFR; the high particle capture efficiency of an N95 FFR must be obtained while minimizing this pressure drop across the media layers. A useful mathematical representation of N95 FFR performance should therefore include accurate expressions for both filter efficiency and pressure drop. In fact, the equations for both of these N95 FFR properties are intertwined because a filter pressure drop equation can be inverted to determine a single, "effective" fiber diameter for use in the filter efficiency model equations despite the filter being comprised of a distribution of fiber diameters (Hinds 1999). Likewise, Brown (1993, pp. 78–79) emphasizes that methods to model capture efficiency due to interception utilize the same assumptions, and related equations, for estimating filter pressure drop. For example, the Kuwabara model to characterize flow around a single fiber (Kuwabara 1959) has been used to model both diffusion and interception particle capture effects (Lee and Liu 1982) as well as filter pressure drop (Pich 1966).

A review of filter efficiency modeling equations applicable to N95 FFRs, with demonstrations of their use, was written by O'Shaughnessy (2022) that can be considered a companion paper to the work described here. Filter modeling equations and related variables described in that paper are referred to extensively in this paper. Although not conducted as an exhaustive systematic review of the topic, O'Shaughnessy suggested that few studies have utilized currently-available N95 FFRs as the basis of comparison for developing filter efficiency mathematical models. In particular, Chen et al. (1993) provide an excellent summary of modeling methods but, having been published three decades ago, does not include current N95 FFRs. Likewise, Balazy et al. (2006) incorporated N95 FFRs like those currently available, but applied an efficiency model that did not use equations to determine the distribution of charges on particles of varying sizes as would be the case for an aerosol encountered in the ambient environment (Hinds, 1999, pp, 335–338).

O'Shaughnessy (2022) discussed the single-fiber efficiency equation for diffusion at length because of its many forms published in the literature, and because that force greatly influences the shape of the left side of the efficiency "dip" as illustrated in Figure S1. The form of the diffusion single-fiber equation also influences the start of the inflection point from ~100% efficiency for the smallest particles to 0% efficiency for larger particles. Although a variety of diffusion equations exist, they are all functions of the inverse of the Peclet number, P_e, which indicates the influence of convective transport relative to diffusive

transport. Likewise, an empirically-derived constant is often applied that has the effect of shifting the inflection point.

Another consideration when modeling the efficiency of an N95 FFR is the value of the charge on the filter fibers. The charge of an N95 FFR fiber with a dipole charge is expressed as a charge per fiber area, C/m^2. This charge is difficult to accurately measure. Buamgartner et al. (1986) describe two methods that require measurements obtained from single fibers viewed microscopically from which they obtained charge levels varying between 224 – 480 $\mu C/m^2$. However, Tabti and colleagues (2009; 2010) developed a system that measured the surface charge from nonwoven sheets of polypropylene with much lower charge levels of 8 and 27 $\mu C/m^2$. Other research groups determined relatively low fiber surface charge levels in the range of 5.1 – 40 $\mu C/m^2$ for polypropylene fibers in filters similar to those used in N95 FFRs by back-calculation to obtain a best-fit of modeled relative to measured efficiencies (Chen et al. 1993; Otani et al. 1993; Chen and Huang 1998). These recent papers, therefore, suggest that current N95 FFRs have surface charge levels in the tens of $\mu C/m^2$, but that hypothesis needs further study.

The theoretical development and use of filter pressure drop models is well described by Brown (1993) who principally relied on the early work by Pich (1966), as does more recent researchers such as Wang et al. (2008). In all cases, the equations are arranged in the format of Equation 1 in which pressure drop, ΔP, is expressed in terms of air dynamic viscosity, μ, air velocity, U_0, filter thickness, L, and fiber diameter, d_f, as well as an empirically-derived function of filter solidity, $f(\alpha)$ (1):

$$\Delta P = \frac{\mu U_0 L}{d_f^2} f(\alpha) \tag{1}$$

To determine $f(\alpha)$, for example, Davies (1953) incorporated all other terms as a dimensionless group (2):

$$\frac{\Delta P d_f^2}{\mu U_0 L} = f(\alpha) \tag{2}$$

and applied a best-fit curve to express $f(\alpha)$ as (3):

$$f(\alpha) = 64\alpha^{1.5}\left(1 + 56\alpha^3\right) \tag{3}$$

Jackson and James (1986) also developed an expression for $f(\alpha)$ based on measurements reported in thirteen other studies as well as their own that has been used in other studies (Higdon and Ford 1996; Koponen et al. 1998; Hosseini and Tafreshi 2010). However, their pressure model is based on fiber radius, r_f, rather than fiber diameter. Jackson and James (1986) also use the dimensionless ratio k/r_f^2, where k indicates the permeability of the media, which is derived directly from Darcy's Law and results in a ratio similar to that shown in the left-hand term of Equation (2) but inverted: $k/r_f^2 = \eta U_0 L/\Delta P r_f^2$. The equation Jackson and James (1986) derived for $f(\alpha)$ in terms of fiber diameter, therefore, results in (4):

$$f(\alpha) = 4\left(\frac{3}{20\alpha}[-\ln(\alpha) - 0.931]\right)^{-1} \quad (4)$$

In Equation 1, d_f is an effective fiber diameter applied to best represent the influence of the entire distribution of fiber diameters within a filter on pressure drop. Light microscopy or electron micrographs have been used to determine the distribution and resulting average fiber diameter (Balazy et al. 2006; Ramirez and O'Shaughnessy 2017) as an estimate of the effective diameter. Another approach is by inverse calculation of Equation 1 to solve for d_f (Hinds 1999). The Davies pressure model (Equations (1) and (3)) has been used for this purpose (Letourneau et al. 1987; Payet et al. 1992). Given that the two commonly-used filter pressure models defined in Equations (3) and (4) in combination with Equation (1) were developed decades ago, there is a need to evaluate their use for predicting the pressure drop of currently available N95 FFRs.

Study Aims

A review of the current literature on mathematical models developed to predict filter efficiency and pressure drop of N95 FFRs indicates a paucity of current research on this topic. The nature of the diffusion equation and the fiber charge value applied to the model are critical elements for correctly modeling filter efficiency, neither of which have been evaluated specifically for currently available N95 FFRs. Likewise, filter pressure drop models developed decades ago are still in use without verification of their applicability to N95 FFRs.

Therefore, the overall goal of this research was to optimize mathematical models developed to predict N95 filter efficiency and pressure drop. The first aim of this research was to create a set of procedures and associated filter attributes that could be used to model the pressure drop of a typical N95 FFR. A second aim was to optimize a model to predict N95 filter efficiency by incorporating the equations described by O'Shaughnessy (2022) together with methods to determine an appropriate diffusion equation and the magnitude of the fiber charge.

METHODS

Filter media characterization

Six N95 FFRs manufactured by three companies in North America were chosen to represent a variety of commercially available N95s. To aid in comparisons between them, all N95s were standard cup-shaped, two-strap FFRs. They included 3M models 8210 and 8511 (St. Paul, MN); Moldex models 2200 and 2300 (Culver City, CA); and Dentec models AD2N95 and AD4N95 (Newmarket, Ontario). An additional set of four filter media consisting of polypropylene or polyester fibers with diameters larger than those occurring in N95s were also evaluated including: Cleer Air Filters model CLEER SNS 85 (Clover, SC); LeSac model PE-1 (Chicago, IL); Superior Felt & Filtration model Technostat 70 Plus (McHenry, IL); and Jo-Ann Stores Blizzard Fleece (Hudson, OH).

Each of the chosen N95 FFRs consisted of multiple layers of nonwoven material of various types and quantities. Therefore, the layer applied to each N95 FFR designed to capture particles (here called the "filtering layer"), consisting of randomly-oriented fibers with a relatively wide range of diameters most commonly produced during the melt-blown process (Bandi 2020), were extracted from a 5-cm circular cut-out of each tested mask. The filtering layer consisted of a single sheet of filter media in the Moldex models and consisted of two sheets of media in all other N95 FFRs. In the case of a double filtering layer, the two layers were analyzed together. All results are associated with the properties of the filtering layer and not of all layers of an N95 FFR.

Filtering layers were evaluated to determine thickness, solidity, fiber diameter and pressure drop. All measurements were made in triplicate. A microscopic method was used to determine thickness. A 1 × 1 × 5 cm wooden block was attached to the long edge of glass slide to allow it to stand on that edge. The filter was cut in a straight line with a razor and propped up on that edge between two of the upright slides on the viewing area of an inverted microscope (CKX31, Olympus Corp., Center Valley, PA). Photos of the cut edge were analyzed digitally using ImageJ (Ver. 146r, NIH, Bethesda, MD) relative to the digital image of a stage micrometer with a resolution of 0.8 μm/pixel. This method attempted to measure filter thickness without applying pressure to the filter as may occur when using calipers.

Filter solidity was obtained by cutting 15.7-mm (5/8-in) diameter samples from a filtering layer using a hole punch. Sample mass, m_f, was measured using a six-place microbalance (Model MT5, Mettler Toledo, Columbus, OH). Given the known surface area of the sample and measured thickness, the sample volume, V, was computed. The filter fibers were assumed to consist of polypropylene having a density, ρ_p, of 0.86 g/cm^3. Filter solidity, α, was then computed as the ratio of the sample density relative to the density of polypropylene (7):

$$\alpha = \frac{m_f/V}{\rho_p} \tag{7}$$

Additional details concerning the measurement of thickness and solidity are given in the thesis by Purdy (2019).

Filter fiber diameters were measured from photos obtained from a scanning electron microscope (SEM, Hitachi S-4800) taken at 500x magnification. One sample was prepared for each filter type from which four images were captured at four randomly selected locations of the sample. ImageJ was used to measure fiber diameter from the digital photos (Figures S2 and S3 of the online supplement) using the 100 μm scale bar associated with each photo to convert pixels to lengths with a resolution of 0.1 μm/pixel. One hundred fibers, chosen using a randomizing system, were sized for each filter type, 25 from each of the four photos per filter sample. A total of 100 fibers measured for each filter was based on guidance developed for counting asbestos fibers (NIOSH, 2019a). Both individual and strand-like fiber bundles were considered a fiber. Although the diameter values were somewhat skewed, the average was considered the best estimate of the central tendency

of all diameters measured as the median underestimated the potential influence of large bundles. Additional details are given in the thesis by Harris (2021).

Filter pressure drop measurement and equation development

During a pressure drop test, a filter sample was held tightly between the upper and lower sections of a 12-cm tall, 5-cm diameter conical column with 2.7-cm inner hole. Figure 1 shows the testing setup for both efficiency and pressure drop testing. During pressure drop testing the aerosol generation system was disconnected from the inlet (top) of the sampling column. Vacuum air was regulated to achieve flow rates through the column of 1.6 and 3.6 L/min, which correspond to face velocities of 4.7 cm/s and 10.5 cm/s, respectively, given the 2.7-cm diameter channel through the column. Previous research (O'Shaughnessy et al. 2021) identified a face velocity of 8 cm/s as typical when testing an N95 FFR at 85 L/min as dictated by the N95 FFR approval process (NIOSH 2019b). Therefore, these flow rates were chosen to span face velocities typically induced during that test. Three filter samples were cut from different respirators for each of the six N95s and each sample tested at both flow rates. This test was also conducted using samples cut out of all filter layers of each N95 FFR to compare pressure drop between the filtering layer and the entire N95.

Pressure drop was measured using a calibrated differential pressure sensor (Dwyer Series 646, Michigan City, IN) with a measuring range of 0 – 64 mm H_2O. Tygon® tubes connected the differential pressure sensor to upstream and downstream ports on the sampling column. The voltage signal from the pressure sensor was measured using LabVIEW 2017 software (National Instruments, Austin TX) every 0.25 s for 25 s. Microsoft Excel was then used to convert the volts to pressure drop (ΔP) in mmH_2O and produce an average of the 100 measurements.

Given measured characteristics for each N95 FFR filtering layer, the initial constant, 64, of Equation (3) was adjusted to minimize the root mean squared error (RMSE) between that model and the dimensionless group given in Equation (2) to obtain a pressure drop model having the general form of the Davies equation derived from the characteristics of the six currently available N95 FFRs. The minimization process was performed using the root-solving function in Excel Solver. The optimized pressure drop equation was then compared to the equations developed by Davies (1953) and Jackson and James (1986), as well as to points created using the four filter media types with large-diameter fibers.

Achieving a best-fit efficiency model

Filter efficiency measurement—To measure the efficiency of the filtering layers from the six N95 FFRs, a testing apparatus was developed to deliver a salt (NaCl) aerosol to the charged filter media. As shown in Figure 1, a nebulizer (Model 3076, TSI Inc., Shoreview, MN) generated a polydisperse salt aerosol from a 2% solution of reagent-grade NaCl. The droplet aerosol passed through a heated steel tube to produce dry salt particles followed by a charge-neutralizer (Model 3088, TSI Inc., Shoreview, MN) to obtain an aerosol with a Boltzmann charge equilibrium. Particles exiting the neutralizer combined with filtered, compressed air to dilute the generated aerosol.

Additional details on this test system are described by O'Shaughnessy et al. (2021). In brief, a 5-cm diameter sample of the filtering layer removed from an N95 FFR was clamped into place between the upper and lower portion of the hollow column used for pressure testing. A scanning mobility particle sizer (SMPS), consisting of an electrostatic classifier (Model 3082, TSI Inc., Shoreview, MN) in combination with a condensation particle counter (Model 3787, TSI Inc., Shoreview, MN), was used to measure the upstream and downstream particle counts from which filter efficiency was calculated. The statistical method established by O'Shaughnessy and Schmoll (2013) was followed to eliminate efficiency values that were based on counts that were too low to reliably use for that purpose. This elimination typically occurred for counts in the lowest-diameter bins because the count distribution of the generated aerosol reached a minimum in that region of particle sizes.

Model using an effective diameter—A filter efficiency model incorporating an effective diameter determined from the average of all fibers measured from each filtering layer was evaluated first. The model was developed in Microsoft Excel. The process for achieving a best-fit model relative to measured efficiency data obtained from the testing apparatus was accomplished in two steps. First, the single-fiber diffusion equation was adjusted to best-fit the efficiency curve using a method described by Wang et al. (2007). As shown in Figure S1, diffusion primarily affects the left side of the total filter efficiency dip, but the dielectrophoretic force ("D-force"), and, to a lesser extent, the Coulombic force ("C-force"), also influences efficiency in that range of the dip. Total single-fiber efficiency, E_{Σ}, in that range was, therefore, assumed to be the sum of the single fiber efficiencies for diffusion, E_D, and the D-force, E_{Di} (6):

$$E_{\Sigma} = E_D + E_{Di} \tag{6}$$

And, given the relationship expressed in Equation 6, E_D can be determined as (7):

$$E_D = -\frac{\pi d_f}{4\alpha L} ln P_f - E_{Di}, \tag{7}$$

where P_f is the total filter particle penetration. Furthermore, Wang et al. (2007) suggested that an empirical model of diffusion single fiber efficiency can be adequately expressed as a power law based on the Peclet number, P_e (8):

$$E_D = b \cdot Pe^m \tag{8}$$

A spreadsheet was then developed to determine the values of constants b and m of Equation (8) by first plotting the measured filter efficiency values for each of the remaining particle diameters analyzed by the SMPS. The efficiency values that formed the decreasing slope on the left side of the efficiency dip were then chosen for further analysis and converted to fractional penetrations. Given a measured P_F value together with measured values of d_f, L and α, Equation (7) was used to determine E_D for each particle diameter while applying Equations (7) and (8) of O'Shaughnessy (2022) to model E_{Di} for each particle diameter. Regression analysis was then applied to determine the coefficient, b and exponent, m, that

best-fit the log of the measured E_D values. Because of the influence of the D-force, the unknown fiber charge value was also adjusted until the r^2 value generated as part of the regression analysis was maximized.

The second step for obtaining a best-fit model to efficiency data was to apply the diffusion equation coefficients obtained in step one to the single fiber diffusion equation associated with a complete filter model that also contains the effects of interception, impaction, gravity, the D-force and the C-force on particle capture while treating the aerosol as having a Boltzmann charge distribution. A complete description of such a model is given in O'Shaughnessy (2022).

Given the measured characteristics of the filter that was tested and the results from the first step, all values needed for the model to best-fit the measured efficiencies had been determined. However, when applying the fiber charge obtained from step one, the model produced slightly higher efficiencies for the large particle diameters than measured efficiencies. As shown in Figure S1, the C-force, which is also influenced by the fiber charge, also has an influence on efficiency for large particles. Therefore, to adjust the fiber charge, the root mean squared error (RMSE) between measured efficiencies and modeled total filter efficiency for particles < 0.1 μm (within the major portion of the dip) was computed across the range of particle diameters measured. The root-solving function in Microsoft Excel, Solver, was then used to minimize the RMSE by adjusting the fiber charge value.

Model using a distribution of fiber diameters—Following the method described by O'Shaughnessy (2022), the efficiency values derived from measurements were also compared to a model in which the filter was assumed to have fiber diameters following a lognormal distribution. In brief, the software package, MATLAB (MathWorks, Natick, MA) was used to incorporate the equations for all forces applied in the Excel model and run a For Loop that determined the filter efficiency at each of the measured particle diameters for 31 fiber diameters in the range of 0.1 – 100 μm spaced evenly on a logscale. Assuming a perfect lognormal distribution, the probability of occurrence of each fiber size was calculated and applied to the computed efficiency values and then summed as given in Equation 19 of O'Shaughnessy (2022). From SEM measurements of fiber diameters (Table S1), the geometric standard deviation (GSD) averaged near 2.0, which was used as a starting value. Although the geometric mean is the central tendency of a lognormal distribution, to compare directly to results obtained when using a single effective diameter equal to the arithmetic average fiber diameter, that average value was used in place of the geometric mean of the fiber diameters when running the model.

Due to the complexity of this approach, a minimum RMSE could not be obtained using a root-solving approach. Therefore, three variables directly influencing the nature of the efficiency curve were adjusted manually to obtain a curve that best matched the measured values; the fiber surface charge, the value of the coefficient, b, of Equation (8) while holding m constant and equal to −2/3; and the GSD. Setting $m = -2/3$ negated the need to alter two variables associated with the diffusion equation, where the value chosen is that which results directly from theory (Lee and Liu 1982).

RESULTS AND DISCUSSION

Application of fiber charge to the model

O'Shaughnessy (2022) described two methods for applying the D- and C-forces to the total filter efficiency equation. One method produces a single dip in efficiency that occurs when both the C-force and D-force are assumed to affect particles of all charge states (Chen et al. 1993; Romay et al. 1998). This is the condition shown in Figure S1. However, a second method produces two dips in efficiency, which occurs if the model is developed under the assumption that the D-force only affects neutral (0 charge) particles (Lathrache and Fissan 1987) and the C-force affects all charged particles. Therefore, whether the D-force is applied to particles of all charge states was investigated prior to this study using techniques that result in filter efficiency measurements under various combinations of charged and uncharged filter and aerosol particles (Kanaoka et al. 1987; Otani et al. 1993; Romay et al. 1998; Yang et al. 2007). The methods and results of that study are provided in the online supplement in the section "Validation of the charge efficiency model". In brief, the results (Figure S9) support the modeling method by which a single dip in efficiency occurs at a single, most-penetrating particle size.

Filter pressure drop measurement and equation development

Measured values for, L, d_f, α and ΔP for each of the six N95 FFR filter layers evaluated during this study and their descriptive statistics are given in Table 1. Filter pressure drop, ΔP, is given at the value computed for a face velocity of 8 cm/s from the slope resulting from the measured velocities when forcing the intercept to zero. Fiber diameter, d_f, is given in Table 1 as the arithmetic mean of the 100 fibers measured for each FFR. Histograms of the fiber diameter distribution and related descriptive statistics are given in Figure S4 and Table S1.

These arithmetic mean fiber diameters were applied to the dimensionless ratio given in Equation (2) as the effective diameter, d_f, together with the measured values for filter thickness, L, as well as constant values for face velocity, U_0 = 8 cm/s, and air dynamic viscosity, $\mu = 1.81 \times 10^{-4}$ g/cm-s, to obtain paired relationships between that dimensionless group and solidity for each filtering layer. The six points derived in that manner are plotted in Figure 2. Those points are also shown in relation to the data published in Jackson and James (1986), which include measurements made in other studies that satisfied the criterion that the flow regime follow Darcy's Law indicated by a Reynold's number, $Re < 10$ ($Re = \rho_a U_0 d_f / \eta$, where ρ_a is air density) and a Knudsen number, $Kn < 0.01$ ($Kn = 2\lambda/d_f$, where λ is the molecular mean free path = 0.0664 μm). Calculation of Re for the six filters at 8 cm/s face velocity resulted in a range of 0.011 – 0.020. However, the Kn range of 0.036 – 0.064 for the six filters is > 0.01 resulting from their small-diameter fibers but are within the slip-flow regime defined as $0.001 < Kn < 0.1$ (Bian et al. 2018). The data points used by Davies (1953) to develop Equation (3) are not shown in Figure 2, but all would plot within those given by Jackson and James (1986).

As can be seen in Figure 2, the six points derived from this study fall outside of the points collected by Jackson and James. Four of the points, corresponding to the 3M and Moldex filter layers form a curvilinear relationship. However, the two Dentec filter points are

removed from that pattern resulting from their lower solidity values. The curves developed by Davies (Equation (3)) and Jackson and James (Equation (4)) are also given in Figure 2. The two curves are very similar throughout the measured range of α but diverge where $\alpha < 0.02$.

The value of the dimensionless group is most sensitive to differences in fiber diameter given that it is a squared term in the numerator of Equation (2). The types of filter media evaluated by both Davies (1953) and Jackson and James (1986) primarily included fabrics with fiber diameters much larger than found in N95 filtering layers. For media evaluated in air, Jackson and James (1986) report fiber diameters in the range of 39 – 193 μm. Characteristics of the four additional filters containing large-diameter fibers (~20 μm) are shown in Table 2. The points obtained from those values are shown in Figure 2, which are generally within the range given by Jackson and James (1986). Therefore, the points derived from N95 filtering layers in this study result from smaller values for the dimensionless group for the same α as points derived from other studies. Given this result, a modified form of the Davies equation (Equation (3)) was warranted to best relate filter pressure drop to solidity using the method in which the constant of Equation (5) was adjusted to minimize the RMSE between equation solutions for each of the six dimensionless groups and their associated values derived from measurements. This procedure resulted in a value of 8.3, which changed Equation (3) to (9):

$$f(\alpha) = 8.3\left(1 + 56\alpha^3\right) \tag{9}$$

that is valid within the range of measured solidity values of $0.05 < \alpha < 0.14$.

The relationship between filtering layer pressure drop and the pressure drop across all N95 layers varied in relation to the number of media layers. The 3M and Dentec N95s have three media layers whereas the Moldex N95s have two layers, which diminished the difference between the filtering-layer and all-layer pressure drop relative to those of the other two brands. Table S2 provides the average pressure drop (of three samples) for both conditions. The overall average increase in pressure drop for both 3M N95s, both Dentec N95s, and both Moldex N95s over that of the corresponding filtering layers was 1.45, 1.24, and 1.08, respectively.

Achieving a best-fit efficiency model

Modeling using an effective fiber diameter—The efficiency model was first validated by applying a single, effective diameter, d_f, equivalent to the arithmetic mean of the fiber diameter distribution for the filtering layer of each N95 FFR. An example of the relationship between Peclet number and the single fiber efficiency resulting from diffusion is shown in Figure 3, which was obtained from the average of three filtering layer efficiency tests using the Moldex 2200 filtering layer. For this example, Equation 8 coefficients of 0.276 and −0.435 for b and m were obtained, respectively. The high r^2 value of 0.988 was typical of those obtained and validates the use of Equation 8 to model single fiber efficiency due to diffusion. Similar results for all six filtering layers tested resulted in an average (standard deviation) of 0.233 (0.075) for b and −0.423 (0.038) for m. All results are provided in Table S3 of the supplement and their averages are shown in Table 3. For the example shown in Figure 3, a surface charge value of 28 μC/m^2 was applied to the equations to determine the

single fiber efficiency due to the dielectrophoretic force that maximized the r^2 value of the linear regression.

The corresponding total filter efficiency model developed from the diffusion equation produced in the first step is given in Figure 4. As an indication of the variability between filter measurements of the same type, all three efficiency measurements of the Moldex 2200 and their average are shown in Figure S5. As shown in Figure 4, the model curve follows the trend of the measurements closely except when modeling the efficiency of the largest particles. For comparison, plots similar to that shown in Figure 4 are given for all six measured filters in Figure S6. For the example shown in Figure 4, the application of the Solver routine to minimize the RMSE resulted in adjusting the surface charge value from 28 $\mu C/m^2$ to 26.6 $\mu C/m^2$ to compensate for the increasing Coulombic force with larger diameter particles (Figure S1). All filtering layer surface charge values resulting from minimizing the RMSE are given in Table S3. The average (standard deviation) surface charge of all six filtering layers was 27.0 (9.3) $\mu C/m^2$ (Table 3).

Modeling using a distribution of fiber diameters—Figure 4 also includes a curve resulting from the application of a lognormal distribution of fiber diameters to the efficiency model. Similar curves for all six filtering layers are given in Figure S6. The RMSE of modeled to measure efficiency values was reduced from 0.0043 when using an effective diameter to 0.0018 when incorporating a distribution of fiber diameters. The improvement in model accuracy was primarily gained from a better fit in the region of large particles > 0.1 μm where efficiency modeled using a fiber distribution better followed the gradual asymptote to unity of the measurements. That pattern is a consequence of the influence of the large-diameter fibers in the distribution that produce lower efficiency than a smaller, single effective diameter.

The average (standard deviation) surface charge of all six filtering layers was 50 (14) $\mu C/m^2$, which was almost twice the value obtained when modeling with an effective diameter (Table 3, with individual results given in Table S4). This result may be explained by the interaction between fiber diameter and fiber charge on efficiency. For the same charge and solidity, larger fiber diameters will produce less efficient filters than small-diameter fibers. The application of a lognormal distribution of fiber diameters skewed toward increasing fiber diameter resulted in a greater influence of the larger diameter fibers than when using a single effective diameter. To compensate, the fiber charge had to be increased to best match the measured efficiency values. Given that the application of a distribution of fiber diameters to the model is a more realistic approach, the higher fiber charge obtained can be assumed to be closer to the actual level.

Other model inputs that affected the shape of the efficiency curve included the diffusion model constant, b, and exponent, m of Equation 9. As expected, increasing the value of b shifted the starting point of the downward inflection of the dip to the right. Decreasing the value of m (more negative) resulted in a steeper decline. Interestingly, choosing a value of $m = -2/3$ effectively represented that decline, which incorporates the combined effect of the entire fiber diameter distribution on efficiency, and differs from the average value of $m = -0.423$ when using a single effective diameter. Lastly, differences in the GSD of the fiber

diameter distribution change the range of particle sizes over which the dip occurred, where an average value of 1.8 resulted in a curve that best fit the range of the measured values (Tables 3 and S3).

N95 Filtering Layer Summary—Assuming that the six N95s chosen for this study represent the variety available in the United States in 2023, then a universal N95 FFR can be proposed with qualities near the average of those measured in this study for use in future studies involving efficiency models of N95 FFRs. Table 1 provides the average of measurements made from the six N95 filtering layers for filter thickness and solidity, and fiber diameter and surface charge. Likewise, averages of fiber charge, the diffusion equation coefficients, and the GSD when modeling a fiber diameter distribution are given in Table 3. However, some slight adjustments to those averages were needed to provide a modeled efficiency curve that best represents the overall average of measured values. Therefore, Tables 1 and 3 also provide suggested filter characteristics values that can be combined in a model that best represents a typical N95. Note that the suggested effective fiber diameter of 2.5 μm derived from the average is also obtained when back-solving Equation (2) for fiber diameter, d_f, and using Equation 9 to solve for $f(\alpha)$ while applying the average values given in Table 1 for thickness, L, and solidity, α, at the average pressure drop, ΔP, of 6.2 mm H_2O (61 Pa) at 8 cm/s face velocity, U_0.

The resulting curves generated when applying an effective diameter and a distribution of fiber diameters is given in Figure 5 in comparison to the average efficiency of all six filtering layers, and related standard deviation, for each particle diameter measured with the SMPS. As illustrated in Figure 5, the curves for the two efficiency models using the suggested input values follows the overall average of efficiency measurements closely with the method involving a distribution of fiber diameters having an RMSE 66% that of the RMSE when using a single effective diameter.

An explanation and results associated with additional model considerations are provided in the supplement. They include an analysis of the minimum number of forces necessary to produce an accurate filter efficiency model, which demonstrates that only diffusion, the D-force and the C-force are necessary (Figure S10). A second analysis considered the use of the Davies equation (Equation 3) to derive an effective diameter for use in the efficiency model. Although numerically possible (Figures S7, S8, S11), both the fiber charge and the constant, b, of Equation 8 must be increased beyond expected levels to compensate for the large fiber diameter predicted by that equation.

CONCLUSION

A filter pressure drop model was developed by modifying a commonly-used equation (the Davies equation) to best represent the pressure drop performance of the filtering layer of currently available N95 FFRs produced in North America. The overall pressure drop through all layers of an N95 FFR increases in the range of 8% – 45% over that of the filtering layer depending on the number of additional media layers.

A filter efficiency model that simulates the capture of particles having a Boltzmann charge distribution by fibers with a dipole charge was validated by comparison to measurements of the particle capture efficiency of six standard, cup-shaped N95 FFRs. Using measurements of the filtering layer solidity, thickness, and fiber diameter, the diffusion equation and the fiber surface charge was altered to produce modeled efficiency values that closely follow the "dip" in efficiency characteristic of N95 FFRs. That dip was demonstrated to be primarily a consequence of the intersection of the waning effect of diffusion and the increasing effect of the dielectrophoretic force, with additional, marginal influence by the Coulombic force.

A model that incorporated the combined effect of a distribution of fiber diameters was shown to follow the right-side, increasing slope of the dip more closely than when using a single "effective" diameter in the model. Two sets of filter characteristics values typical of current N95 FFRs are provided that produce an efficiency curve using either the effective fiber diameter approach or the fiber distribution approach. Future work will involve the use of those values in models for the purpose of optimizing filter performance while minimizing pressure drop.

Supplementary Material

Refer to Web version on PubMed Central for supplementary material.

FUNDING

This research was supported by the University of Iowa Environmental Health Sciences Research Center (NIH P30 ES005605), and by the Heartland Center for Occupational Health and Safety, a NIOSH/CDC Education and Research Center (T42OH008491).

DATA AVAILABILITY

All data created as part of this research is available upon request from the corresponding author. All filter efficiency models produced as a result of this study, in either Excel or MATLAB, are available upon request of the corresponding author.

REFERENCES

Balazy A, Toivola M, Reponen T, Podgorski A, Zimmer A, Grinshpun SA. 2006. Manikin-Based Performance Evaluation of N95 Filtering-Facepiece Respirators Challenged with Nanoparticles. Ann Occup Hyg. 50(3):259–269. [PubMed: 16344291]

Bandi M 2020. Electrocharged facepiece respirator fabrics using common materials. Proceedings of the Royal Society A. 476(2243):20200469.

Baumgartner H, Loffler F, Umhauer H. 1986. Deep-bed electret filters: the determination of single fiber charge and collection efficiency. IEEE Trans Dielectr Electr Insul. (3):477–486.

Bergman M, Zhuang Z, Brochu E, Palmiero A. 2015. Fit assessment of N95 filtering-facepiece respirators in the US Centers for Disease Control and Prevention Strategic National Stockpile. J Int Soc Respir Prot. 32(2):50. [PubMed: 26877587]

Bian Y, Zhang L, Chen C. 2018. Experimental and modeling study of pressure drop across electrospun nanofiber air filters. Build Environ. 142:244–251.

Brown RC. 1993. Air filtration: an integrated approach to the theory and applications of fibrous filters. Oxford: Pergamon.

Chen CC, Huang SH. 1998. The effects of particle charge on the performance of a filtering facepiece. Am Ind Hyg Assoc J. 59(4):227–233. [PubMed: 9586197]

Chen CC, Lehtimaki M, Willeke K. 1993. Loading and filtration characteristics of filtering facepieces. Am Ind Hyg Assoc J. 54(2):51. [PubMed: 8452097]

Davies CN. 1953. The seperation of airborne dust and particles. Proceedings of the Institution of Mechanical Engineers. 167(1b):185–213.

Fukakusa J, Rosenblat J, Jang B, Ribeiro M, Kudla I, Tarlo S. 2011. Factors influencing respirator use at work in respiratory patients. Occup Med. 61(8):576–582.

Harris Z 2021. Adjusting a Commonly Used Respirator Pressure Drop Equation for Use with Modern Respirators. Iowa City, IA: The University of Iowa.

Higdon J, Ford G. 1996. Permeability of three-dimensional models of fibrous porous media. J. Fluid Mech 308:341–361.

Hinds WC. 1999. Aerosol Technology: Properties, Behavior, and Measurement of Airborne Particles. Vol. 2nd. New York: John Wiley & Sons. Book, Whole.

Hosseini S, Tafreshi HV. 2010. Modeling permeability of 3-D nanofiber media in slip flow regime. Chem Eng Sci. 65(6):2249–2254.

Jackson GW, James DF. 1986. The permeability of fibrous porous media. CJCE. 64(3):364–374.

Kanaoka C, Emi H, Otani Y, Iiyama T. 1987. Effect of Charging State of Particles on Electret Filtration. Aerosol Sci Tech. 7(1):1–13.

Koponen A, Kandhai D, Hellen E, Alava M, Hoekstra A, Kataja M, Niskanen K, Sloot P, Timonen J. 1998. Permeability of three-dimensional random fiber webs. PRL. 80(4):716.

Kuwabara S 1959. The forces experienced by randomly distributed parallel circular cylinders or spheres in a viscous flow at small Reynolds numbers. JPSJ. 14(4):527–532.

Lathrache R, Fissan H. 1987. Enhancement of particle deposition in filters due to electrostatic effects. Filtr Sep. 24(6):418–422.

Lee KW, Liu BYH. 1982. Theoretical Study of Aerosol Filtration by Fibrous Filters. Aerosol Sci Technol. 1(2):147.

Letourneau P, Mulcey P, Vendel J. 1987. Effect of dust loading on the pressure drop and efficiency of HEPA filters. Filtr Sep. 24(4):265–267.

NIOSH. 2019a. Asbestos and other fibers by PCM. NIOSH Manual of Analytical Methods. 7400(3). [Internet] https://www.cdc.gov/niosh/nmam/pdf/7400.pdf.

NIOSH. 2019b. Determination of Particulate Filter Efficiency Level for N95 Series Filters against Solid Particulates for Non-Powered, Air-Purifying Respirators Standard Testing Procedure. Procedure No. TEB-APR-STP-0059, Revision 3.2.

O'Shaughnessy PT, Schmoll LH. 2013. Particle count statistics applied to the penetration of a filter challenged with nanoparticles. Aerosol Sci Technol. 47(6):616–625. [PubMed: 24678138]

O'Shaughnessy PT. 2022. Review and demonstration of equations applied to models of filtering facepiece respirator particle capture efficiency. J Occup Environl Hyg. 19(10–11):615–628.

O'Shaughnessy PT, Strzelecki B, Ortiz-Hernandez M, Aubin P, Jing X, Chang Q, Xiang J, Thorne PS, Stapleton JT. 2021. Characterization of performance and disinfection resilience of nonwoven filter materials for use in 3D-printed N95 respirators. Journal Occup Environ Hyg. 18(6):265–275.

Otani Y, Emi H, Mori J. 1993. Initial collection efficiency of electret filter and its durability for solid and liquid particles [translated]. KONA Powder Part. J 11:207–214.

Payet S, Boulaud D, Madelaine G, Renoux A. 1992. Penetration and pressure drop of a HEPA filter during loading with submicron liquid particles. J Aerosol Sci. 23(7):723–735.

Pich J 1966. Pressure drop of fibrous filters at small Knudsen numbers. Ann Occup Hyg. 9(1):23–27. [PubMed: 5900990]

Purdy M 2019. Comparison of Facemask Characteristics with User Assessment of Comfort. Iowa City, IA: The University of Iowa.

Ramirez JA, O'Shaughnessy PT. 2017. Filter penetration and breathing resistance evaluation of respirators and dust masks. J Occup Environ Hyg. 14(2):148–157. [PubMed: 27676311]

Romay FJ, Liu BY, Chae S-J. 1998. Experimental study of electrostatic capture mechanisms in commercial electret filters. Aerosol Sci Tech. 28(3):224–234.

Shaffer RE, Janssen LL. 2015. Selecting models for a respiratory protection program: what can we learn from the scientific literature? AJIC. 43(2):127–132.

Tabti B, Dascalescu L, Plopeanu M, Antoniu A, Mekideche M. 2009. Factors that influence the corona charging of fibrous dielectric materials. J Electrostat. 67(2–3):193–197.

Tabti B, Mekideche M, Plopeanu M, Dumitran L, Herous L, Dascalescu L. 2010. Corona-charging and charge-decay characteristics of nonwoven filter media. IEEE Trans Ind Appl. 46(2):634–640.

Wang J, Chen DR, Pui DYH. 2007. Modeling of filtration efficiency of nanoparticles in standard filter media. J Nanopart Res. 9(1):109–115.

Wang J, Kim SC, Pui DYH. 2008. Figure of merit of composite filters with micrometer and nanometer fibers. Aerosol Sci Tech. 42(9):722–728.

Yang S, Lee W-MG, Huang H-L, Huang Y-C, Luo C-H, Wu C-C, Yu K-P. 2007. Aerosol penetration properties of an electret filter with submicron aerosols with various operating factors. J Environ Sci Health A. 42(1):51–57.

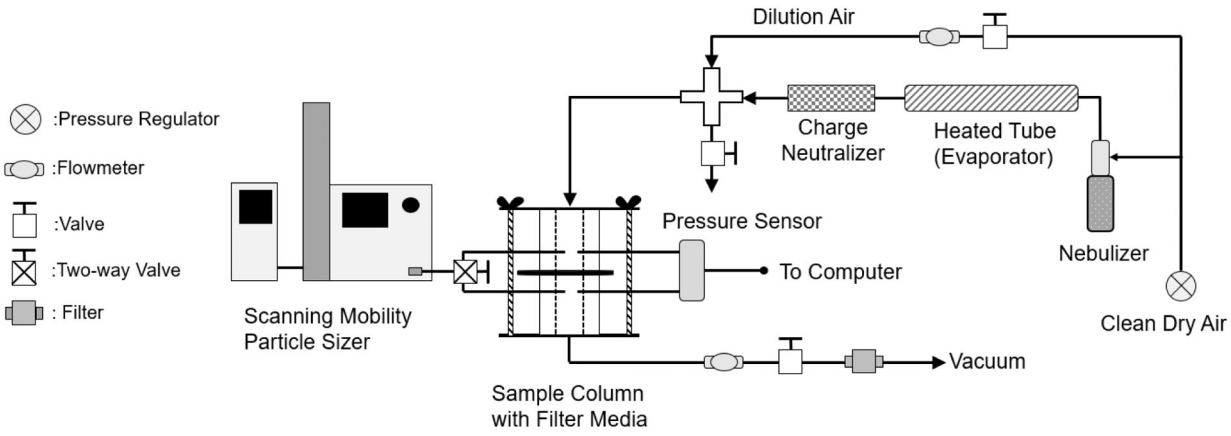

Figure 1.
Schematic of the filtering layer efficiency and pressure testing system.

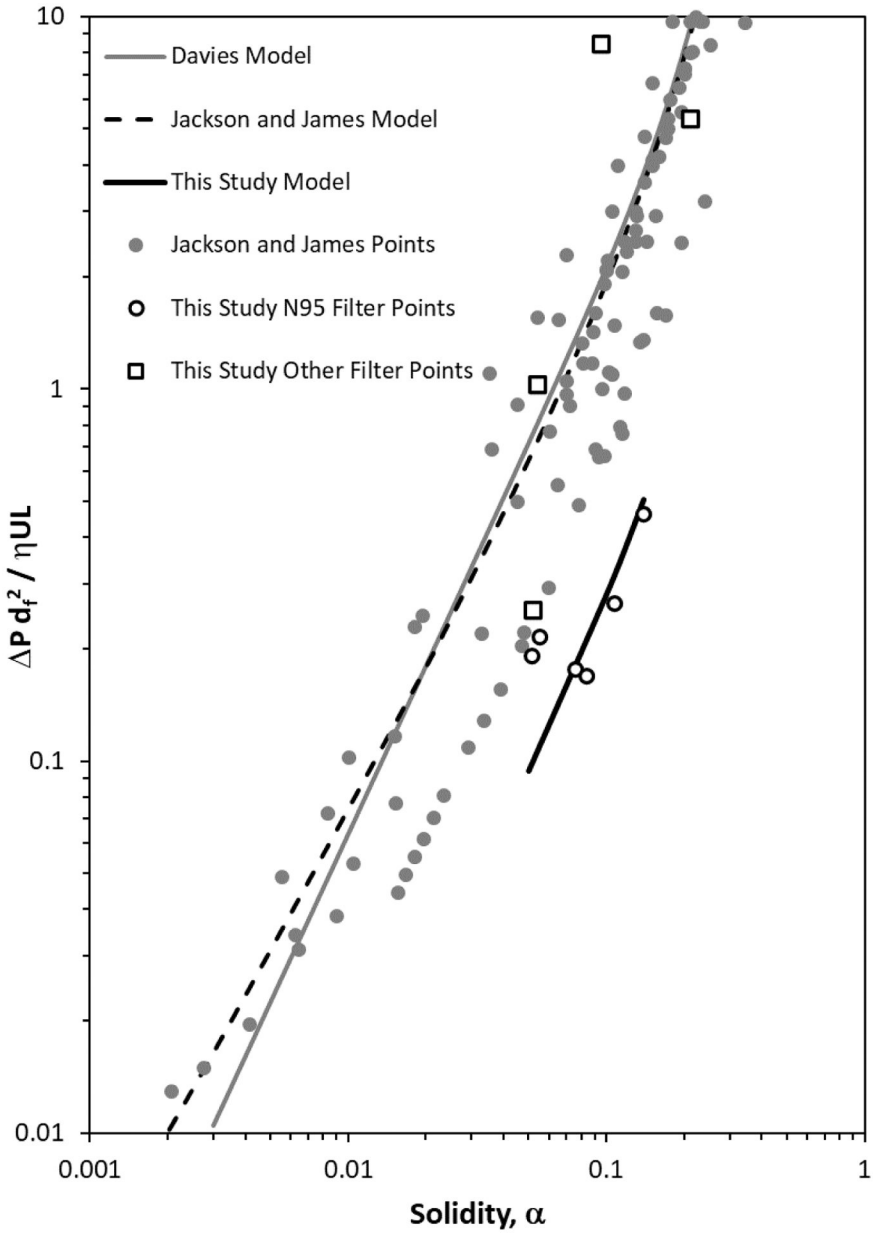

Figure 2.

Modeled relationships between the dimensionless pressure parameter and filter solidity given by Davies (1953), Jackson and James (1986), and this study. Plotted points include those given in a table by Jackson and James (1986) and those produced during this study using N95 filtering layers and filters having larger diameter fibers.

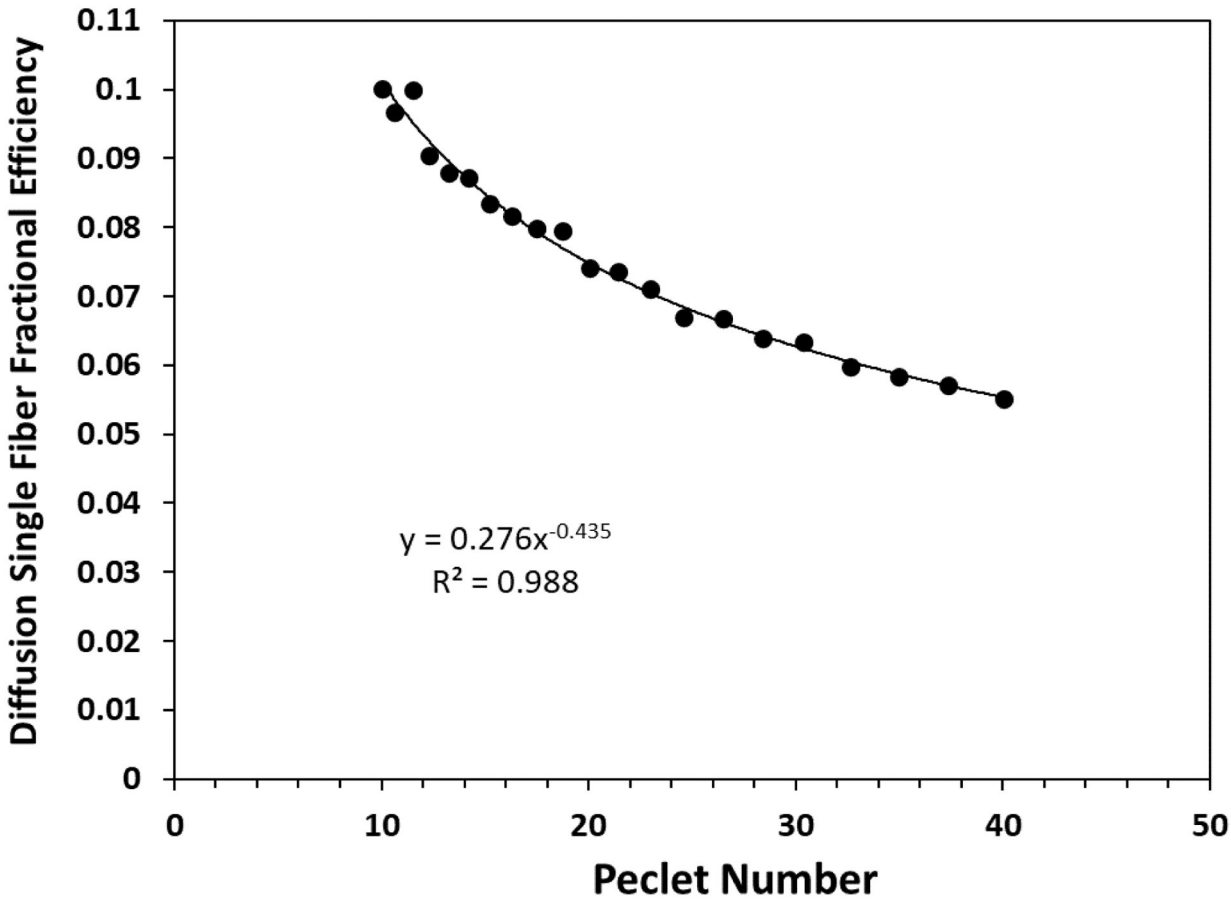

Figure 3.

Measured and modeled relationship between the Peclet number and the single-fiber efficiency resulting from diffusion. The points represent the average of three measurements made using the Moldex 2200.

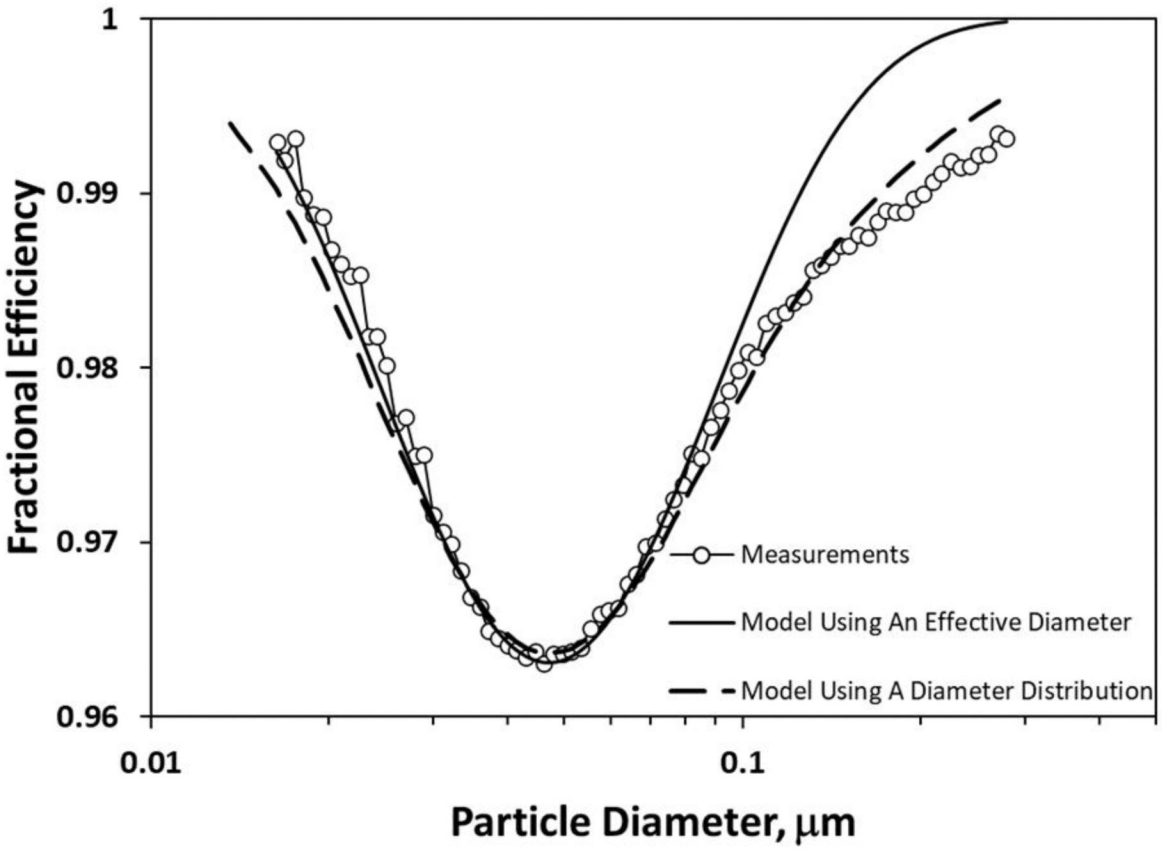

Figure 4.
Measurements and modeled total efficiency curves of the Moldex 2200 filtering layer. The modeled curves utilized either an effective diameter or a distribution of fiber diameters.

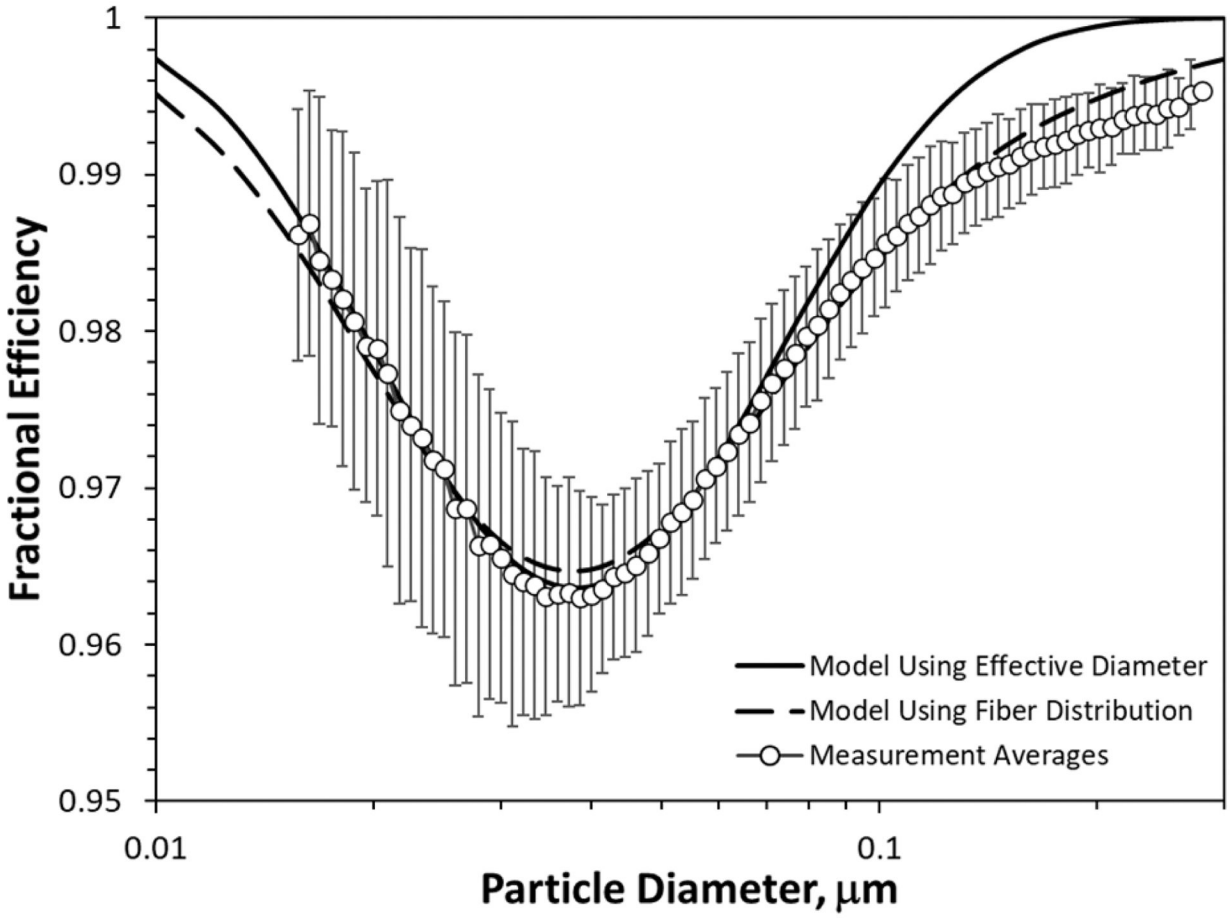

Figure 5.

Measured efficiency values with error bars (standard deviation) averaged across all six N95 filtering layers assessed in this study. The corresponding total efficiency curves incorporating either an effective diameter or a distribution of fiber diameters are also shown and utilized filter characteristics given as suggested values in Tables 1 and 3.

Table 1.

Measured N95 filtering layer characteristics and suggested values for modeling a typical N95 filtering layer.

N95 Filtering Layer	Thickness cm	Fiber Diameter μm	Solidity	Pressure Drop[1] mm H_2O
3M 8210	0.176	3.0	0.076	5.14
3M 8511	0.154	3.1	0.084	3.97
Moldex 2200	0.084	2.6	0.107	6.67
Moldex 2300	0.065	2.1	0.139	7.63
DenTec AD2N95A	0.095	2.3	0.052	5.22
DenTec AD4N95	0.133	2.2	0.055	8.67
Average	0.118	2.5	0.086	6.22
Standard Deviation	0.043	0.4	0.033	1.74
Suggested for Model	0.120	2.5	0.085	

[1]Pressure drop at a face velocity of 8 cm/s.

Table 2.

Measured filter media characteristics.

Filter Media	Thickness cm	Fiber Diameter μm	Solidity	Pressure Drop[1] mm H_2O
CLEER SNS 85	0.129	22.1	0.096	2.72
PE-1	0.280	23.4	0.211	4.04
Technostat 70 Plus	0.170	15.3	0.054	1.06
Blizzard Fleece	0.333	11.7	0.052	0.93

Table 3.

Derived filter characteristics and suggested values for modeling a typical n95 filtering layer.[1]

Condition	Fiber Charge μC/m^2	Diffusion Constant	Diffusion Exponent	Fiber Diameter GSD
Single Effective Diameter				
Average	27.0	0.233	−0.423	
Standard Deviation	9.3	0.075	0.038	
Suggested for Model	23.5	0.190	−0.420	
Diameter Distribution				
Average	50	1.03	−0.667	1.8
Standard Deviation	14	0.25	--	0.1
Suggested for Model	45	0.90	−0.667	1.8

[1]Other modeling conditions include face velocity = 8 cm/s, particle density = 2.16 g/cm^3 for NaCl, dielectric constant of the particle = 5.9 for NaCl, and = 2.2 for polypropylene fibers, and applying an aerosol with a Boltzmann charged distribution.